CARBON 52 (2013) 193–200

Available at www.sciencedirect.com

SciVerse ScienceDirect

journal homepage: www.elsevier.com/locate/carbon

Control of microstructural heterogeneities in carbon nanotube foams

Jordan R. Raney, Richard Y. Wang, Chiara Daraio *

Division of Engineering and Applied Science, California Institute of Technology, 1200 E. California Blvd. MC 105-50, Pasadena, CA 91125, USA

ARTICLE INFO

Article history:
Received 17 April 2012
Accepted 10 September 2012
Available online 18 September 2012

ABSTRACT

Arrays of aligned carbon nanotubes (CNTs) under compression are known to exhibit a dissipative hysteretic response similar to classical foams. Here, we control the microstructure of the arrays during synthesis using a variable supply of carbon source and catalyst. We control CNT alignment and density along the array height, creating bands of high- and low-density regions. We study the dynamic response of these materials and show the ability to tailor the location and extent of strain localization under compression. We show that the synthesis procedures described herein allow for construction of CNT arrays with improved protection and energy dissipation in impact tests.

1. Introduction

Arrays of aligned carbon nanotubes (CNTs) have been observed to present a dissipative, hysteretic response under compression, much like open cellular foams [1]. In addition to dissipating significantly more energy during compressive deformation than commercial polymeric foams of comparable density (0.15–0.35 $g cm^{-3}$) [2], these materials are also thermally and electrically conductive and have therefore been proposed as multifunctional millimeter-scale low-density protective layers [1,2]. These systems have received much attention for being functionally graded in their as-synthesized state, possessing variations in such properties as average CNT diameter [3], density [4], alignment [5], presence of contamination [6], and defect density [7] along their height. When these structures are subjected to compression along the long CNT axes these gradients in structural properties are associated with strain localization and sequential collapse [1,8]. More specifically, as an array undergoes increasing compressive strain it proceeds through a sequence of buckling events in which each buckle is completely formed prior to the formation of a new buckle, with the non-buckling region undergoing no apparent deformation [9]. This buckling is observed to take place from the base, defined as the side nearest the growth substrate, where the density also is lowest [4,9]. Such functionally graded properties are often challenging to obtain in macroscopic systems, but are a desirable feature for foams used for protection against impact [10]. Graded properties can improve a material's resistance to damage [11] and are frequently observed in natural systems [12]. The aforementioned graded structure of arrays of CNTs is therefore an interesting feature that may allow such materials to serve as low-density protective foams. Limited low energy impact tests have been performed in the past and shown that similar systems undergo nonlinear deformation and exhibit energy dissipation during impact [13,14]. Here we devise a simple method to further control the deformation and dissipation properties of CNT arrays, which has not been previously reported.

Vapor phase (or "floating catalyst") thermal chemical vapor deposition (CVD) allows for the production of large quantities of millimeter-scale well-aligned CNTs on unmodified, inexpensive quartz surfaces [15]. The low-density (0.15–0.35 $g cm^{-3}$) CNT arrays that result can be repeatedly compressed to large strains (>0.8) and hysteretically recover nearly completely [16]. The microstructure and the resulting bulk mechanical properties of these systems have been

* *Corresponding author.*
E-mail address: daraio@caltech.edu (C. Daraio).
0008-6223/$ - see front matter
http://dx.doi.org/10.1016/j.carbon.2012.09.020

shown to be tailorable to some extent. For example, the choice of hydrogen concentration used in the flow gas during synthesis affects the average CNT diameter as well as the bulk density and resulting mechanical properties of the array [17]. In another study it was shown that partially-graphitic layers of pyrolyzed carbon can be formed around the CNTs, greatly increasing both the bulk density and the stiffness of the array [18]. Others have combined CNT arrays with other materials to affect overall structural properties, either by infiltrating CNT arrays with polymer [19] or nanoparticles [20], or by incorporating them into multilayer structures [2,14,21].

These studies on tailoring CNT arrays tend to focus on understanding and engineering the bulk physical properties of millimeter-scale arrays of CNTs through uniformly modifying the microstructure. While some work has been done to heterogeneously alter the microstructure of CNT arrays [5,22], no work to date has examined how this could be used to affect the mechanical response of the arrays. Here, we introduce microscale heterogeneities during the synthesis process by varying the input rate of catalyst and carbon precursor solution during sample growth. We observe that these heterogeneities can be arranged to tailor compressive strain localization along the height of the array and thereby improve impact energy dissipation.

2. Experimental

2.2.1. *Synthesis of CNT arrays*

A floating catalyst thermal chemical vapor deposition system was used to synthesize the CNT arrays. Specifically, we synthesized millimeter-scale arrays of CNTs on thermally oxidized Si substrates using a CVD system in a flow of argon at 827 °C. As reported in detail elsewhere [17], we typically use a 0.02 g ml^{-1} solution of ferrocene (Fe catalyst precursor) in toluene (carbon source), at an input rate of approximately 0.8–1 ml min^{-1}; however, in this study, we used non-constant input rates for the precursor solution, controlled by a programmable syringe pump. As described in the main text, higher input rates corresponded to lower density regions of CNT growth. This fact was used to synthesize CNT arrays of different architectures, as discussed.

2.2.2. *Quasistatic mechanical deformation*

We designed a small steel vise to hold the CNT arrays at various strains for desired intervals. This allowed for imaging with scanning electron microscope (SEM), in this case using a FEI Quanta 200F at 30 kV. Other cyclic quasistatic compression tests were performed using a commercial materials test system (Instron E3000) at a strain rate of 0.01 s^{-1} to a maximum strain of 0.8, with strain being defined as the total displacement normalized by the total height of the sample (i.e., samples compressed to 0.8 strain are only 20% of their original height at maximum strain).

2.2.3. *Impact tests*

A steel sphere of 3/8 inch diameter and mass 3.47 g was dropped from heights of 3–15 cm onto samples synthesized using different feed rate profiles. Samples used for testing were 1.05 ± 0.10 mm in thickness and 0.287 ± 0.044 g cm^{-3} in bulk density. Though samples of a wider range of heights (0.6–1.4 mm) and bulk densities (0.15–0.35 g cm^{-3}) were synthesized, only those near to the height and density specified above were used in the analyses, in order to avoid introducing additional variables that are known to affect the mechanical response of the CNT arrays [17]. The testing apparatus was activated with a switch that simultaneously triggered a solenoid to release the striker and started a Phantom V12.1 high-speed camera recording at 20 kHz (Fig. 4a). This recorded the motion of the striker throughout the impact event, and allowed calculation of its restitution coefficient using image correlation routines. The apparatus included a force sensor (PCB Piezotronics) underneath the sample, which was activated by the onset of dynamic force as a result of the striker's impact. A computer was used to record the resulting voltage–time data during impact, and voltage was mapped to force using the manufacturer's and our own calibration data.

3. Results and discussion

When high injection rates (several ml min^{-1}) are used in bursts of a few minutes or less we observe that a corresponding softer region results in the final CNT structure. Using high resolution scanning electron microscopy (SEM) (see, for example, the images and similar analysis presented in Ref. [17]) we observe that the CNTs in these softer regions have a lower average diameter than the CNTs in regions synthesized with slower injection rates (~30 nm for the former and ~43 nm for the latter), but have statistically similar areal densities (as estimated by a count of the number of CNTs per unit length across the structure). This narrowing of CNT diameter with increasing injection rate of precursor solution has been observed previously [23,24]. At the other extreme, the precursor input rate can be set to zero by pausing the injection system, depriving the heating zone simultaneously of any new carbon or catalyst. If the system is starved of precursor solution in this way, higher density regions of lateral entanglement (poor CNT alignment) arise [5,22]. Supporting Information Fig. S1 provides an image from the transition region between adjacent bright and dark regions, in which the change in alignment and entanglement can be seen. Past work has quantitatively confirmed the variations in alignment in similar samples [5].

An input rate profile corresponding to a particular CNT growth cycle is shown in Fig. 1a, in which a typical constant input rate of 0.8 ml min^{-1} is used (the normal growth or "control" case for the purposes of this work). In contrast, a variable input rate profile is shown in Fig. 1b, in which the input rate alternates between "excess" (8 ml min^{-1}) and "starvation" (0 ml min^{-1}). Scanning electron microscope (SEM) images corresponding to each case are shown in Fig. 1c and d, respectively. Note the uniform, aligned arrangement of the former, corresponding to the constant input rate, and the distinct horizontal bands of the latter, corresponding to an input rate varying between excess and starvation.

As is typical for arrays of CNTs synthesized using floating catalyst techniques [1,14,16,17], these arrays recover to most

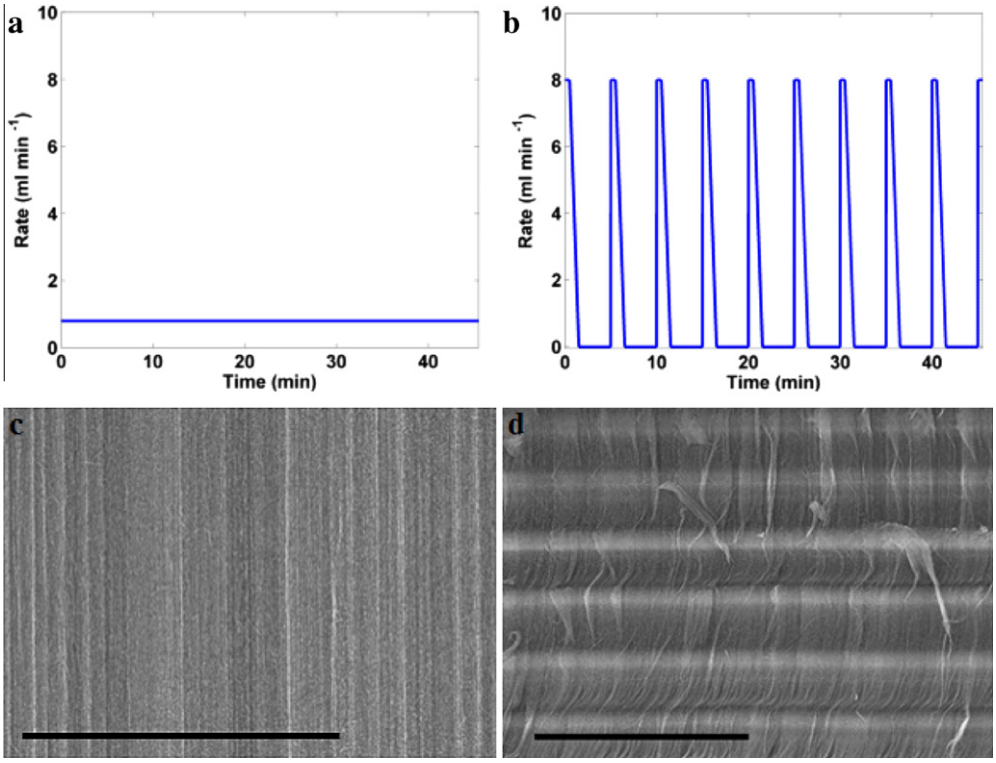

Fig. 1 – The input solution for synthesis of the CNTs consists of 0.02 g ml^{-1} ferrocene in toluene, which can be applied at a constant rate, as in (a), or at a variable rate, such as in (b); the constant input rate displayed in panel *a* corresponds to the uniform, aligned microstructure displayed via SEM in (c) (scale bar is 100 μm) and the cyclic input rate represented in panel *b* corresponds to the banded microstructure displayed in (d) (scale bar is 200 μm).

of their original height even after large quasistatically-applied compressive strains (see Supporting Information Figure S2 for representative stress–strain data measured in quasistatic compression). In order to observe the manner of collapse in the system under compression, we used a steel vise to hold the arrays in a compressed state during SEM imaging. Fig. 2a shows an array corresponding to the input rate profile given in Fig. 1b in the uncompressed steel vise. Fig. 2b shows the same CNT array compressed by the vise to approximately 0.35 strain. Fig. 2c and d give higher resolution SEM images of the uncompressed and compressed states, respectively, from the same sample. It is evident from the changes in Fig. 2d relative to Fig. 2c that the compressive strain is predominantly localized in the dark bands. Comparing the height of the dark band in Fig. 2d to its height in Fig. 2c, as indicated by the vertical dashed lines, shows that the local strain in this particular dark band is about 0.42, about 20% higher than the global strain for the full CNT array of 0.35 (we ensured that we were measuring the same band in both cases by counting the number of bands from the top or bottom of the sample—an important consideration given that there can be small variations in height from one band relative to another).

Additional samples were synthesized with different carbon/catalyst solution input rate profiles. For the simplest cases, samples were synthesized with only one of the low-density bands described above. This was accomplished by using a three-part input rate profile using the programmable syringe pump. The three steps (I–III) are depicted in Fig. 3a: (I), a typical constant input rate of 0.8 ml min^{-1} was used; (II), a higher constant input rate of 5 ml min^{-1} was used in order to provide carbon/catalyst in excess (for 2 min in most cases); and (III), the same constant input rate as in step I (0.8 ml min^{-1}) was used. Notice that due to our synthesis approach, the ramp down time from a high injection rate to a lower injection rate is not instantaneous. This results from a small pool that forms at the front of the furnace (see the later discussion about this point). Two main categories of samples were synthesized: The first category of samples was synthesized with a pause in the precursor input rate between steps I/II and between steps II/III. These samples are referred to as the "discrete" band case because of the sharp boundaries that resulted between the low-density band and the rest of the structure (see Fig. 3a). The other category of samples was synthesized with no pauses between the three steps and is therefore referred to as the "continuous" case due to the lack of apparent sharp boundaries between the low-density band and the rest of the structure (see Fig. 3b).

Other groups have synthesized banded CNT arrays by starting and stopping the injection of the solution of carbon source and catalyst [25] or by dropwise synthesis [25,26]. In these studies, however, the layers were found to separate easily [25]. In our case we find that there is excellent continuity and adhesion between layers for both our discrete and continuous cases. This was quantified by testing the samples in tension along the direction of nominal CNT alignment (see Supporting Information Fig. S3 for a diagram of the setup).

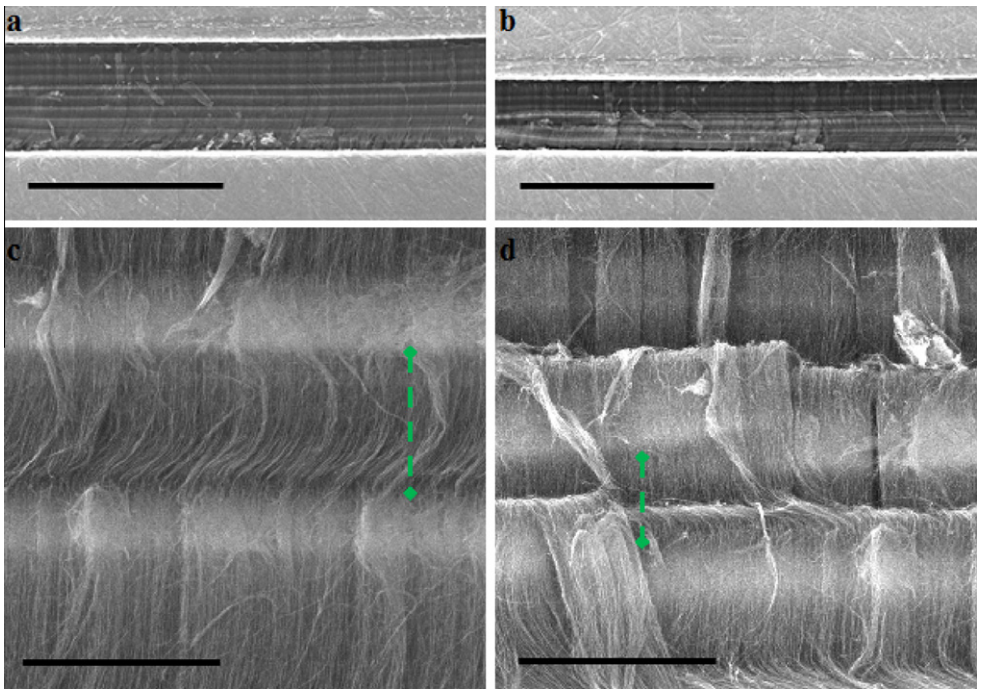

Fig. 2 – (a and b) A banded CNT structure (as synthesized according to the input profile displayed in Fig. 1b) in a steel vise in uncompressed and compressed states, respectively (scale bars are 1 mm); (c and d) the microstructure in the uncompressed and compressed states, respectively (scale bars are 50 μm), revealing how the buckling takes place predominantly in the darker, more aligned regions; the vertical dashed lines are visual aids for observing the strain localization taking place in a particular band.

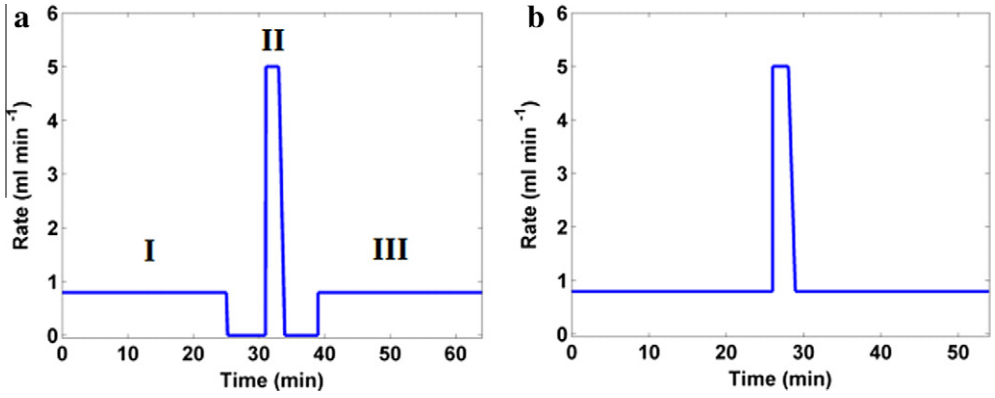

Fig. 3 – (a) The input rate of the precursor feedstock as a function of time that is used for synthesis of a single "discrete" band and (b) the same for a "continuous" band that does not have the same noticeably sharp boundaries.

This is in agreement with an earlier report for a fixed catalyst system using a pulsed carbon source to synthesize sub-micron size bands [22]. Two factors are likely to promote improved continuity and adhesion even in the discrete case. First, rather than abruptly shutting off the injection of precursor solution, some residual evaporation of precursor continues for roughly half a minute (or up to 1 min when a high injection rate has been utilized) due to the buildup of a small pool of precursor in our system directly in front of the heating zone of the furnace. This would act as a buffer to allow for a gradual halt to CNT growth (allowing some CNTs to continue growing for a short time, ultimately bridging separated layers). This also explains why the higher density regions, e.g., as pictured in the SEM image in Fig. 2c, have a gradient in brightness as a function of height. Second, rather than pausing the system for 10–15 min [5,25] or even longer [27], as others have done, we kept the precursor flow off for only a few minutes at a time. If we completely stopped the input of the precursors for more than 10–15 min then the layers readily separated even with light handling. Thus the continuity of the CNTs between layers (and, as a result, the interlayer strength) depends on the time that the structure is deprived of precursors.

By changing the relative times for step I and step III illustrated in Fig. 3a (i.e., the normal synthesis rate before and after the low density band, respectively), the ultimate location

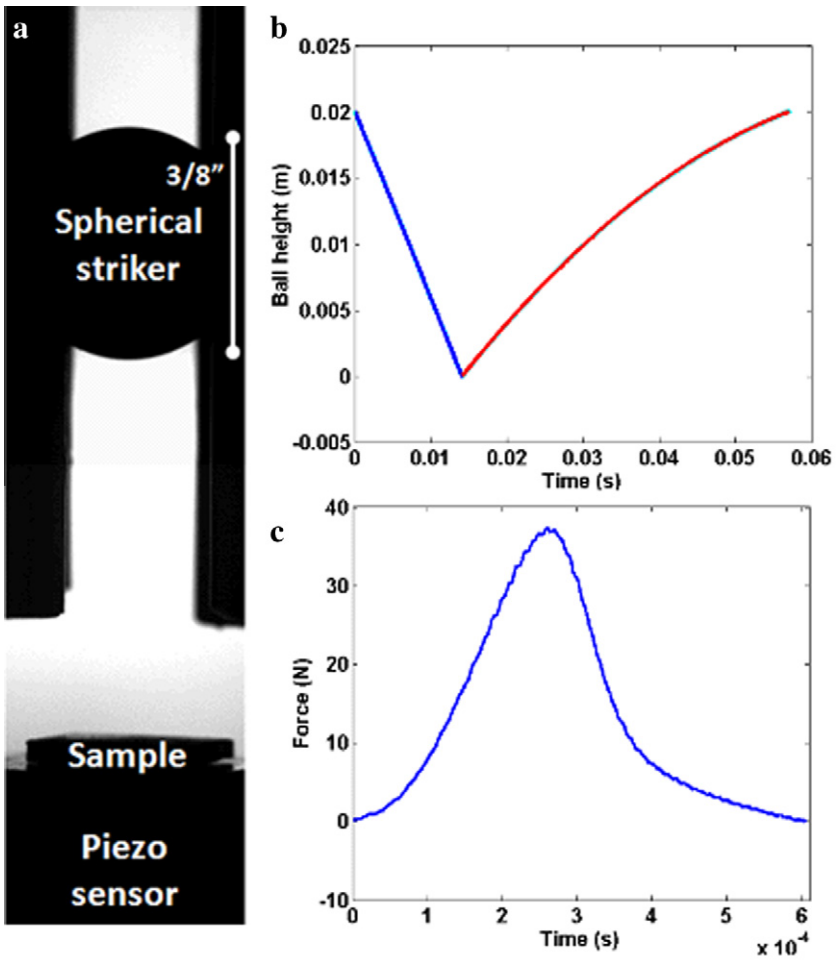

Fig. 4 – (a) A frame taken from the high speed camera with labels indicating the striker, sample, and force sensor; (b), a representative plot of the trajectory of the spherical striker, as extracted from a series of hundreds of sequential images similar to that seen in a; (c) a representative force–time curve extracted from the piezo sensor during a typical test.

of the low-density region could be adjusted along the height of the CNT array. This allowed for the control of where, along the height of the structure, the strain was localized during compression. Note that because of the bottom-up synthesis mechanism of floating catalyst CNTs [5,27], periods of excess precursor solution that occur earlier during synthesis correspond to low-density regions higher on the structure (further from the substrate). Other input rate profiles were used to construct samples with multiple low-density bands (by repeating steps II and III in the above scheme multiple times), samples with low-density bands of different thicknesses (by varying the length of time for step II above), and samples with increased discreteness between low-density and normal-density regions (by varying the amount of time that the input of precursor solution was paused between steps I/II and between steps II/III above).

In addition to the quasistatic observations (i.e., the SEM images in Fig. 2 and the stress–strain data presented in Supplementary Information Fig. S2), impact tests were performed in order to study the dynamic response of these systems (Fig. 4) using a similar technique as in previous work [13,14]. The testing apparatus was activated with a switch that simultaneously triggered a solenoid to release the striker and started a high-speed camera recording at 20 kHz (Fig. 4a). The falling striker was imaged continuously by the camera before, during, and after impact, allowing the calculation of the striker's trajectory (e.g., Fig. 4b) and its incoming and outgoing velocities. The apparatus included a force sensor underneath the sample, activated by the onset of dynamic force as a result of the striker's impact. This gives a force–time profile for each test (e.g., Fig. 4c).

By knowing the incoming and outgoing velocities of the striker, the difference between the kinetic energy of the striker immediately before impact and that immediately after was readily calculated. By the requirements of energy conservation, this difference in kinetic energy for each collision represents the amount of energy dissipated during impact. The percent of incoming striker kinetic energy that was dissipated in each test was used as a figure of merit for the different types of samples. Fig. 5a compares the average amount of striker kinetic energy dissipated as a result of impact for "control" samples (constant precursor input rate of 0.8 ml/min), "discrete" samples (input profile given in Fig. 3a), and "continuous" samples (input profile given in Fig. 3b). Both types of modified samples dissipate significantly more energy than the control case and show only a small difference

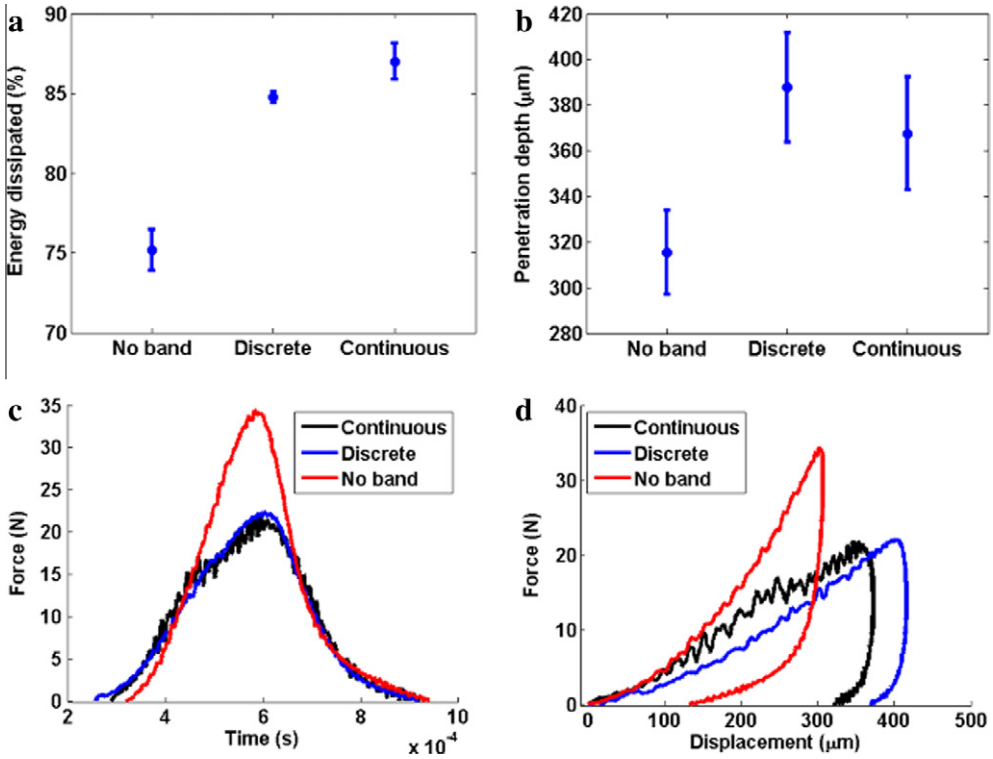

Fig. 5 – (a) Average energy of the striker that is dissipated during an impact test (drop height 12.25 cm) for samples with no bands (the control case), one "discrete" band with sharp boundaries, and one "continuous" band with gradual boundaries; (b) average penetration depth of the striker for the test and sample types in *a*; (c) representative force–time curves for the three sample types; (d) representative force–displacement data for the same.

relative to one another. Though Fig. 5a corresponds to impact events from drop heights of 12.25 cm, we did not see any dependence on striker velocity within the margin of uncertainty of our tests for the drop heights used (from ~3 cm to ~15 cm, corresponding to impact velocities of 0.77–1.72 $m\,s^{-1}$ and approximate initial strain rates at contact of 0.73×10^3–$1.64 \times 10^3\ s^{-1}$).

The low-density regions act to improve impact energy dissipation in multiple ways. First, the low-density bands result in larger displacement during contact. This is illustrated in Fig. 5b, where the average penetration depth during contact of the spherical striker into the sample is given for each sample type. The penetration depth was calculated using the force–time data from the piezo sensor (e.g., Fig. 5c) and the Newtonian equations of motion for the striker. That is, the data for force as a function of time gathered at the sensor is approximated as the instantaneous force on the impacting sphere (ignoring the effects of stress-wave propagation as a first order approximation). Striker velocity as a function of time is determined by integrating this data in Newton's second law, using the incoming velocity of the striker as determined by the high speed camera as the integration constant corresponding to the initial velocity. Finally, this is integrated once more to obtain displacement as a function of time, with the initial position (onset of force) defined as zero position. The striker displacement into the samples is ~20–30% higher for the samples with bands than for those without (Fig. 5b). This increased displacement means that the force during impact acts over a longer distance, with a larger portion of the structure deforming and thereby dissipating energy. This has been shown to be an important cause of energy dissipation in other structures with variations in density, such as functionally-graded honeycombs [28]. Accordingly, the trend for energy dissipation (Fig. 5a) closely matches that for penetration depth (Fig. 5b). Fig. 5d plots representative force–displacement curves for the different types of samples, revealing that the enhanced energy dissipation for the banded samples corresponds to lower peak forces (an important metric for protecting objects behind a foam layer from impact) and higher displacements.

A second contribution to energy dissipation that results from the low-density bands is a slight increase in localized permanent deformation in samples containing them. This was confirmed with SEM imaging after the impact tests (see the permanent deformation for a banded sample pictured in Supplementary Information Fig. S4; this was not observed for the control samples). This was also confirmed by repeated impact events in the same location for each sample, which revealed that after the first one or two impact events the sample performance quickly declines (as concluded by decreased energy dissipation and increased peak force), becoming approximately the same as the control samples'. In this way the softer region appears to become somewhat compacted, losing its benefit after a few strikes (but always performing at least as well as the control samples despite this). It is important to note that this compaction is highly localized. If the striker impacts a portion of the sample even a couple millimeters from a previous impact site then dissipation proceeds as if

the sample had not been impacted previously. The locality of damage is apparent in Fig. S4a, in which the computed maximum penetration depth (e.g., as discussed in the context of Fig. 5b) was used to display the location of the spherical striker (thin dotted curve) at maximum depth. This shows how much of the CNT array came into contact with the striker, and allows one to visualize how these relate to the area of damage.

In addition to the effect on impact energy dissipation that arises from increased striker displacement and sample permanent deformation, we also expect the bands to have a third effect due to resulting changes in stress wave propagation. It has been observed in other systems with layers of varying densities that these can greatly affect stress-wave propagation in high (blast loading) [29] and moderate (low kinetic energy impact tests such as ours) [30] strain rate conditions. Depending on how the stress wave amplitude compares to the local yield stress, the variations in density can result in changes to both the shape of the stress wave as well as the net energy dissipated [31]. This may be a factor in our systems but it requires further study to understand its relative importance, as little has been reported regarding stress wave propagation in aligned CNTs. Given the high correlation of improvement in energy dissipation with penetration depth (Fig. 5a and b, respectively), we expect that increases in penetration depth play the largest role in the increase in energy dissipation at the tested strain rates.

We also studied how the thickness of the band affects the mechanical performance by changing the amount of time during synthesis that the high input rate of precursor solution was used (i.e., step II in Fig. 3a). The resulting samples were tested under impact, and the band sizes were determined using SEM (all samples in this case were of discrete type in order to facilitate accurate measurement of band height). The results are given in Fig. 6. Note that for very short or very thick bands the performance of the samples under impact actually becomes worse than the control case. The best performance is found for bands in the 30–55 μm range. We expect that the optimal band size could vary if strain rate changed significantly, since the density profile for optimal energy dissipation can change with the amplitude of the stress wave [31]. It is also worth noting that some samples of the continuous type performed better than the maximum performance given in Fig. 6, dissipating up to 20% more energy than the control case. Such tests were not included due to the difficulty of accurately measuring the band thickness in the continuous case.

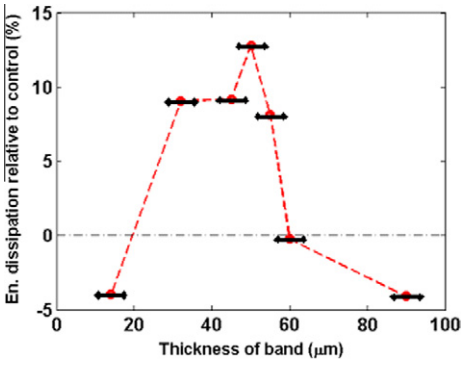

Fig. 6 – The thickness of the low density band affects the energy dissipation of the structure under impact (the horizontal line at 0 indicates the average performance of samples with no bands); the horizontal bars indicate the uncertainty of the band thickness due to variations within any given sample.

4. Summary

By varying the input rate of the precursor solution (containing both the carbon source and the catalyst precursor necessary for CNT synthesis) into a CVD furnace, CNT arrays can be synthesized with a heterogeneous structure. Higher precursor input rates lead to softer regions (with lower average CNT diameter, increased alignment, and less lateral entanglement), which are observed to buckle earlier than higher-density regions when the structure is subject to compression. As a result, strain can be controllably localized in a compressed CNT array. The presence of these low-density regions leads to improved energy dissipation under impact but also tends to increase the permanent deformation or damage that results from such an event. Despite this, even after damage has occurred the samples with the low-density regions still perform at least as well as control samples. We found that impact energy dissipation is dependent on the thickness of these low-density bands. The number of bands is also expected to affect the mechanical performance, but we did not produce a sufficient number of samples of the proper height and density to statistically verify this with our experiments.

Acknowledgements

The authors thank Prof. Jinkyu Yang for his support with the impact tests and Lauren C. Montemayor for her assistance with the assembly of the synthesis apparatus. This work is supported by the Institute for Collaborative Biotechnologies, under contract W911NF-09-D-0001 with the Army Research Office. JRR also gratefully acknowledges support from the Department of Defense via a National Defense Science and Engineering Graduate (NDSEG) fellowship.

Appendix A. Supplementary data

Supplementary data associated with this article can be found, in the online version, at http://dx.doi.org/10.1016/j.carbon.2012.09.020.

REFERENCES

[1] Cao AY, Dickrell PL, Sawyer WG, Ghasemi-nejhad MN, Ajayan PM. Super-compressible foamlike carbon nanotube films. Science 2005;310(5752):1307–10.
[2] Misra A, Raney JR, De Nardo L, Craig AE, Daraio C. Synthesis and characterization of carbon nanotube-polymer multilayer structures. ACS Nano 2011;5(10):7713–21.

[3] Li X, Zhang X, Ci L, Shah R, Wolfe C, Kar S, et al. Air-assisted growth of ultra-long carbon nanotube bundles. Nanotechnology 2008;19:455609.
[4] Pushparaj VL, Ci L, Sreekala S, Kumar A, Kesapragada S, Gall D, et al. Effects of compressive strains on electrical conductivities of a macroscale carbon nanotube block. Appl Phys Lett 2007;91:153116.
[5] Pinault M, Pichot V, Khodja H, Launois P, Reynaud C, Mayne-L'Hermite M. Evidence of sequential lift in growth of aligned multiwalled carbon nanotube multilayers. Nano Lett 2005;5(12):2394–8.
[6] Abbaslou RM, Soltan J, Dalai AK. The effects of carbon concentration in the precursor gas on the quality and quantity of carbon nanotubes synthesized by CVD method. Appl Cat A-Gen 2010;372(2):147–52.
[7] Chakrabarti S, Gong K, Dai L. Structural evaluation along the nanotube length for super-long vertically aligned double-walled carbon nanotube arrays. J Phys Chem C 2008;112(22):8136–9.
[8] Yaglioglu O. Carbon nanotube based electromechanical probes. PhD Thesis. Cambridge, MA, USA: Massachusetts Institute of Technology; 2007.
[9] Hutchens SB, Hall LJ, Greer JR. In situ mechanical testing reveals periodic buckle nucleation and propagation in carbon nanotube bundles. Adv Func Mater 2010;20(14):2338–46.
[10] Sun G, Li G, Hou S, Zhou W, Li W, Li Q. Crashworthiness design for functionally graded foam-filled thin-walled structures. Mater Sci Eng A 2010;527(7–8):1911–9.
[11] Suresh S. Graded materials for resistance to contact deformation and damage. Science 2001;292(5526): 2447–51.
[12] Miserez A, Schneberk T, Sun C, Zok FW, Waite JH. The transition from stiff to compliant materials in squid beaks. Science 2008;319(5871):1816–9.
[13] Daraio C, Nesterenko VF, Jin S. Highly nonlinear contact interaction and dynamic energy dissipation by forest of carbon nanotubes. Appl Phys Lett 2004;85(23):5724–6.
[14] Misra A, Greer JR, Daraio C. Strain rate effects in the mechanical response of polymer-anchored carbon nanotube foams. Adv Mater 2009;21(3):334–8.
[15] Andrews R, Jacques D, Rao AM, Derbyshire F, Qian D, Fan X, et al. Continuous production of aligned carbon nanotubes: a step closer to commercial realization. Chem Phys Lett 1999;303(5–6):467–74.
[16] Suhr J, Victor P, Ci L, Sreekala S, Zhang X, Nalamasu O, et al. Fatigue resistance of aligned carbon nanotube arrays under cyclic compression. Nat Nanotechnol 2007;2(7):417–21.
[17] Raney JR, Misra A, Daraio C. Tailoring the microstructure and mechanical properties of arrays of aligned multiwall carbon nanotubes by utilizing different hydrogen concentrations during synthesis. Carbon 2011;49(11):3631–8.
[18] Li X, Ci L, Kar S, Soldano C, Kilpatrick SJ, Ajayan PM. Densified aligned carbon nanotube films via vapor phase infiltration of carbon. Carbon 2007;45(4):847–51.
[19] Ci L, Suhr J, Pushparaj V, Zhang X, Ajayan PM. Continuous carbon nanotube reinforced composites. Nano Lett 2008;8(9):2762–6.
[20] Raney JR, Zhang H-L, Morse DE, Daraio C. In situ synthesis of metal oxides in carbon nanotube arrays and mechanical properties of the resulting structures. Carbon 2012;50(12):4432–40.
[21] Raney JR, Fraternali F, Amendola A, Daraio C. Modeling and in situ identification of material parameters for layered structures based on carbon nanotube arrays. Compos Struct 2011;93(11):3013–8.
[22] Jackson JJ, Puretzky AA, More KL, Rouleau M, Eres G, Geohegan DB. Pulsed growth of vertically aligned nanotube arrays with variable density. ACS Nano 2010;4(12):7573–81.
[23] Maghrebi M, Khodadadi AA, Mortazavi Y, Rahimi M, Sane A, Tsakadze Z, et al. The effects of carrier gas and liquid feed flow rates on longitudinal patterns of CNT growth. Mater Chem Phys 2010;124(2–3):1139–45.
[24] Tapasztó L, Kertész K, Vértesy Z, Horváth ZE, Koós AA, Osváth Z, et al. Diameter and morphology dependence on experimental conditions of carbon nanotube arrays grown by spray pyrolysis. Carbon 2005;43(5):970–7.
[25] Deck CP, Vecchio KS. Growth of well-aligned carbon nanotube structures in successive layers. J Phys Chem B 2005;109(25):12353–7.
[26] Cao A, Zhang X, Wei J, Li Y, Xu C, Ji L, et al. Macroscopic three-dimensional arrays of fe nanoparticles supported in aligned carbon nanotubes. J Phys Chem B 2001;105(48):11937–40.
[27] Li X, Cao A, Jung YJ, Vajtai R, Ajayan PM. Bottom-up growth of carbon nanotube multilayers: unprecedented growth. Nano Lett 2005;5(10):1997–2000.
[28] Ajdari A, Nayeb-Hashemi H. Dynamic crushing and energy absorption of regular, irregular and functionally graded cellular structures. Int J Solids Struct 2011;48(3–4):506–16.
[29] Wang E, Gardner N, Shukla A. The blast resistance of sandwich composites with stepwise graded cores. Int J Solids Struct 2009;46(18–19):3492–502.
[30] Cui L, Kiernan S, Gilchrist MD. Designing the energy absorption capacity of functionally graded foam materials. Mater Sci Eng A 2009;507(1–2):215–25.
[31] Kiernan S, Cui L, Gilchrist MD. Propagation of a stress wave through a virtual functionally graded foam. Int J Non-linear Mech 2009;44(5):456–68.